

Magnetotransport and dielectric properties of perovskite ruthenate and titanate thin films

J. H. Hao,^{1,a)} Z. H. Wang,² and J. Gao³

¹*Department of Applied Physics and Materials Research Centre, The Hong Kong Polytechnic University, Hong Kong, People's Republic of China*

²*National Laboratory of Solid Microstructures, Department of Physics, Nanjing University, Nanjing 210093, People's Republic of China*

³*Department of Physics, The University of Hong Kong, Hong Kong, People's Republic of China*

(Received 11 August 2007; accepted 27 January 2008; published online 21 March 2008)

Perovskite thin films of conductive ferromagnetic SrRuO₃ and incipient ferroelectric SrTiO₃ were epitaxially grown by laser molecular beam technique. The magnetotransport properties of ferromagnetic films were measured by applying the magnetic field within a wide temperature range. We have observed magnetization hysteresis and significant anisotropic magnetotransport behaviors of thin films. The low-frequency dielectric properties of SrTiO₃ films were studied. It is found that the microstructures and strain in films may strongly affect the magnetotransport and dielectric properties of perovskite oxides. © 2008 American Institute of Physics. [DOI: 10.1063/1.2899957]

I. INTRODUCTION

Perovskite thin films are of scientific and technological interest since these materials exhibit a wide range of physical properties ranging from insulating to semiconducting to superconducting, from paramagnetic to ferromagnetic, and from paraelectric to ferroelectric.¹ Among a wide range of perovskite oxide materials, SrTiO₃ (STO) has an ABO₃ structure with alternating layers of SrO (A-site plane) and TiO₂ (B-site plane). The surface of STO can be terminated by SrO or TiO₂. Because of chemical and structural compatibility of many perovskite oxides to STO, all-oxide systems such as STO/SrRuO₃ (SRO)/LaAlO₃ (LAO) are very attractive for various device applications. Perovskite ruthenate SRO has widely been used in capacitors and ferroelectric devices with all-oxide structures as an electrode, due to its excellent chemical stability and electrical conductivity.^{2,3} SRO crystallizes in the *Pbma* orthorhombic structure with lattice parameters $a=0.5567$ nm, $b=0.5553$ nm, and $c=0.7845$ nm. SRO can also be regarded as a GdFeO₃-type pseudocubic perovskite structure and a bulk lattice parameter of 0.393 nm, which is much closer to the lattice parameter of STO ($a_{\text{STO}}=0.3905$ nm). In addition, SRO is an itinerant ferromagnet with a Curie temperature $T_C \sim 160$ K.⁴ Recent studies demonstrated that the integrated system of STO and SRO is particularly useful not only for the understanding of materials properties but also for the development of novel devices.⁵⁻⁷

Here, we present epitaxial structures of SRO/LAO and STO/SRO/LAO prepared by laser molecular beam epitaxy (MBE), which combines the advantages of pulsed laser deposition for oxide film growth and of MBE for single-crystal film growth. We demonstrate the effects of temperature and magnetic field of epitaxial SRO thin films on their

electrical transport properties. Furthermore, the dielectric properties of STO thin films grown on SRO/LAO are shown.

II. EXPERIMENTS

The SRO and STO films were grown in a laser MBE system.^{8,9} Briefly, a ceramic SRO target and a single-crystal STO target were used to grow SRO and STO films, respectively. A KrF excimer laser (wavelength of 248 nm) was employed in a repetition rate of 5 Hz. The LAO substrate was heated to 770 °C. To form a parallel-plate capacitor structure for dielectric measurements, a 350 nm thick SRO was first deposited on LAO to serve as a bottom electrode, and subsequently the STO film was deposited on the SRO layer. The deposited films were cooled to room temperature in an oxygen atmosphere of 600 mbars. Finally, a top Ag electrode was thermally evaporated onto the STO thin films.

The epitaxial growth of the films was analyzed by x-ray diffraction (XRD) analysis. The surface morphology of thin films was examined by a scanning probe microscope (SPM) using a dynamic force mode. The properties of electrical transport in the films were measured by a standard four-probe method. Magnetotransport properties of SRO thin films were performed on a commercial physical property measurement system (Quantum Design, Inc.). Dielectric properties of STO films were measured using an Agilent 4284A Precision LCR meter with option adding ± 40 V internal dc bias voltages. The bias voltage dependence of the capacitance and dielectric loss ($\tan \delta$) was measured in a closed-cycle cryogenic system, allowing for a continuous temperature sweep within the temperature range from 10 to 300 K. The measurements were performed at 1 kHz with a signal level of 0.2 V_{rms}.

III. RESULTS AND DISCUSSION

Figure 1 shows the XRD results of STO/SRO/LAO system. In the θ - 2θ scan of the films [Fig. 1(a)], only the (00l) peaks of the STO are present along with SRO buffer layer (in

^{a)}Author to whom correspondence should be addressed. Electronic mail: apjhao@polyu.edu.hk.

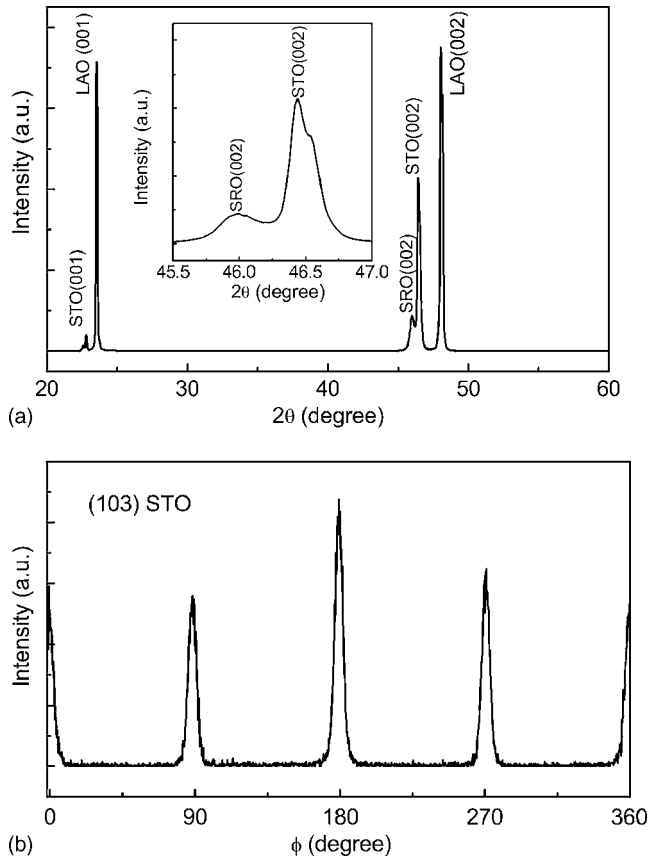


FIG. 1. XRD for the system of STO/SRO/LAO: (a) the θ - 2θ scan. The inset shows the detailed pattern of STO and SRO; (b) the ϕ scan using (103) for the STO peak.

the pseudocubic notation) and LAO substrate. It demonstrates that the STO films grow with c axis normal to the SRO/LAO. The SRO crystal structure is indexed with a pseudocubic unit cell with lattice parameter of 0.393 nm in Fig. 1(a). The STO film in the structure of STO/SRO/LAO is expected to be under tensile strain as the lattice parameter of STO is smaller than the pseudocubic lattice parameter of SRO. The STO peak could be separated from the SRO peak as shown in the inset of detailed pattern. The in-plane epitaxial alignment of the films was investigated by the ϕ scan of the STO (103) peak. Only four peaks, 90° apart, are observed for the STO films in Fig. 1(b). This indicates that the STO film is in plane aligned with the SRO/LAO.

Figure 2 shows the temperature and magnetic field dependence of electrical resistance R of SRO films at $H=0$ and 2 T with $\mathbf{H}\parallel c$. It indicates that the SRO thin films show metallic behavior from 10 K to room temperature. It is noted that there is a change of slope at the T_C of the film, indicating a ferromagnetic ordering at about 140 K. Such a behavior is similar to those reported by other researchers.^{4,10} However, the transition occurs at lower temperatures in the SRO film compared to that in corresponding single crystal. It suggests that the strain and defect in our SRO films possibly suppress the Curie temperature.

We measured the electrical resistance (R) of SRO films at different temperatures as a function of the applied field \mathbf{H} . As shown in Fig. 3, the strong hysteresis in R was observed in the films with $\mathbf{H}\parallel c$ axis below ferromagnetic transition

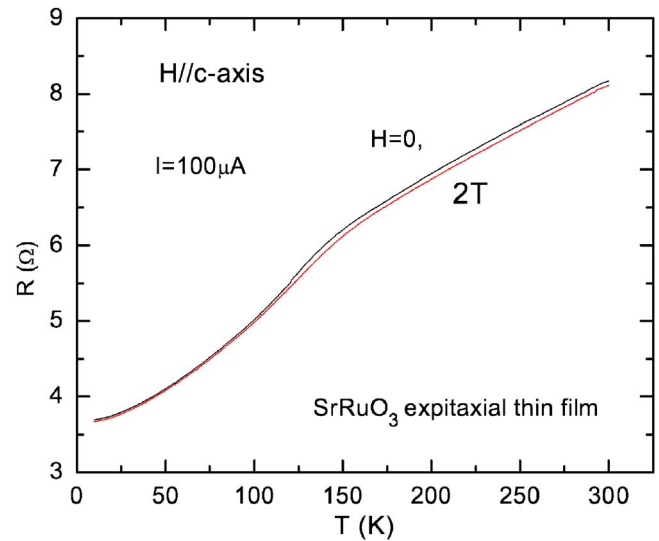


FIG. 2. (Color online) Temperature dependence of the resistance of SRO thin films at $H=0$ and 2 T with $\mathbf{H}\parallel c$ axis.

temperature. In particular, the hysteresis is pronounced at lower temperatures, and it becomes smaller with an increase in temperature. Above T_C , no hysteresis in SRO resistance was found. It is apparent that the hysteresis can only be observed in the ferromagnetic state of SRO. Consequently, the hysteretic effect in Fig. 3 was possibly due to the magnetization hysteresis. The peak in the hysteresis corresponds to the coercive field and the point of overlap between the forward and backward sweeps of the field corresponds to the saturation field. As the temperature increases up to T_C , the coercive field is reduced as observed in Fig. 3.

Moreover, the magnetotransport measurement was performed as a function of the angle θ between \mathbf{H} and c axis in the films with different applied magnitudes of \mathbf{H} at $T = 10$ K. As seen in Fig. 4, the value of R varies with θ for all values of magnetic field \mathbf{H} . The minimum value of R occurs when \mathbf{H} is perpendicular to c axis, i.e., $\theta=90^\circ$. The results exhibit strong dependence of electrical transport not only on the angle between \mathbf{H} and c axis of the films but also on the magnitude of H . Therefore, the observation demonstrates significant anisotropic magnetotransport behaviors in SRO thin films. Magnetotransport properties are likely to be related to the microstructures of ferromagnetic perovskite oxides such as carrier scattering due to the thermally fluctuating spins or the spin-disorder scattering. When the induced magnetic moment is developed, the amplitude of the spin fluctuation decreases so that the resistivity of materials decreases.¹¹ Theoretical study on the SRO films revealed that coherent distortions of the oxygen octahedron network may determine the stability of the magnetic moment on the Ru ion. The structural and magnetic parameters exhibit substantial changes, allowing one to discuss the role of symmetry and possibilities of magnetostructural tuning of SRO-based thin-film structures.¹²

Figure 5 shows SPM image of SRO thin film grown on LAO substrate. The morphology of the film indicated that the strain due to the large lattice mismatch promoted the growth in three dimensional island growth mode. The pioneering

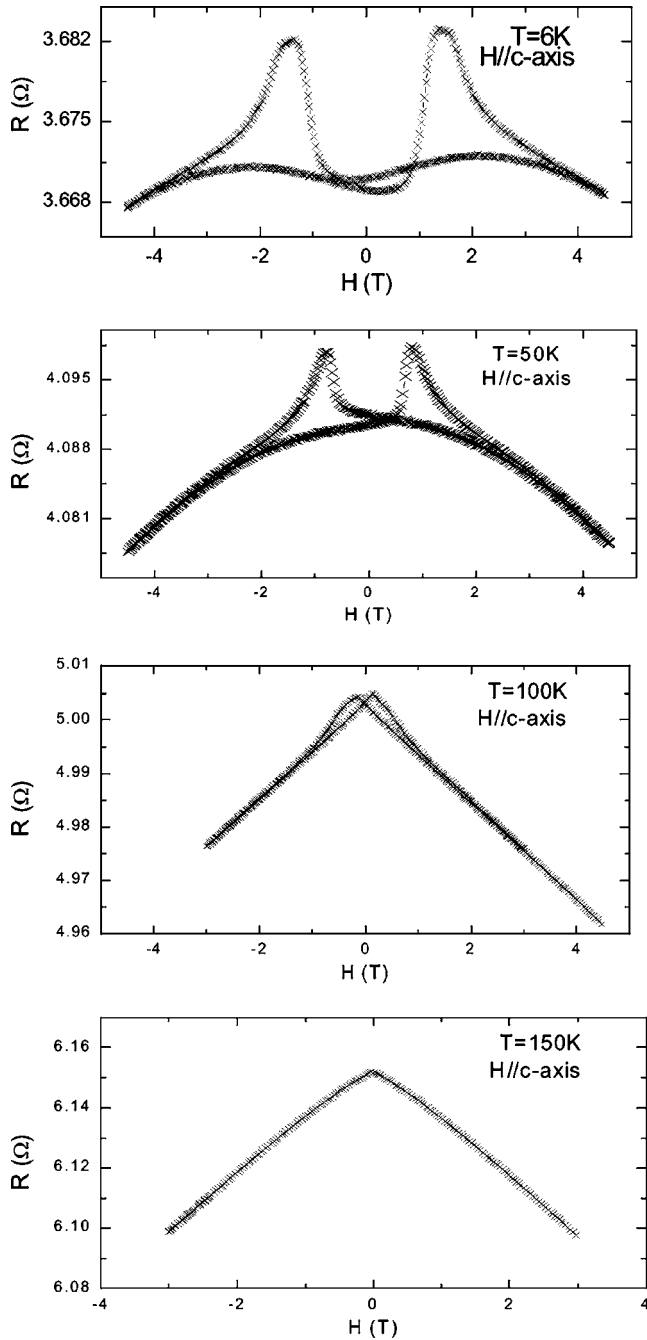


FIG. 3. Magnetic field dependence of the resistance of SRO films at different temperatures.

work of Jiang *et al.* indicated that the microstructures of SRO films are composed of two types of 90° rotational domain structures.¹³ Each type of domain has an in-plane orientation relationship with respect to the substrate. Antiphase boundaries were observed within each domain structure. Kacedon *et al.* found that the presence of 90° domains in the plane results in identical magnetotransport properties within the plane.¹⁴ However, it seems that the formation of domain orientations in SRO thin films has little effect on the anisotropic magnetotransport behaviors of out of plane. In addition, our previous studies indicated that the misfit between the SRO layer and the LAO substrate is mainly accommodated by partial dislocations in SRO thin films from the mea-

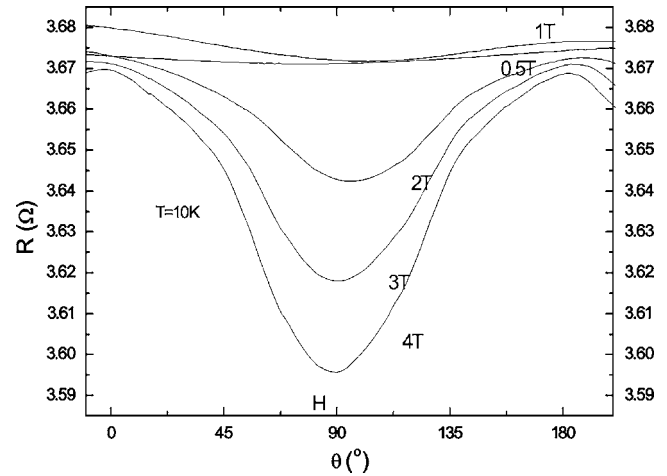


FIG. 4. Resistance of SRO films at $T=10$ K as a function of angle between H and c axis for different magnitudes of H .

surements of high-resolution transmission electron microscopy (HRTEM).^{15,16} In fact, many previous studies reported by other groups demonstrated that the magnetotransport properties of SRO thin films at low temperature are affected by their strain, misfit dislocations, and microstructure.^{17,18}

Figure 6 shows the low-frequency dielectric constant (ϵ) and dielectric loss tangent ($\tan \delta$) as a function of measuring temperature for STO films grown on SRO/LAO. Overall, the STO films show the dielectric properties differing substantially from those in corresponding single-crystal materials. The ϵ value of STO films increases as the temperature decreases. However, as most reported STO films, here the low-temperature ϵ is much lower than the value of single-crystal STO (over 10^4) at low temperature. The mechanism responsible for the small dielectric constant in thin films compared to the single-crystal value at low temperature has been investigated in our earlier reports.^{19,20} In addition to the phenomenon caused by a “dead layer” of very low dielectric constant between the STO film and the electrode, the dramatic reduction of the dielectric constant has been attributed to a profound change of the reduced softening of its lowest optical-phonon mode in STO films.

On the other hand, the value of loss in STO thin films is

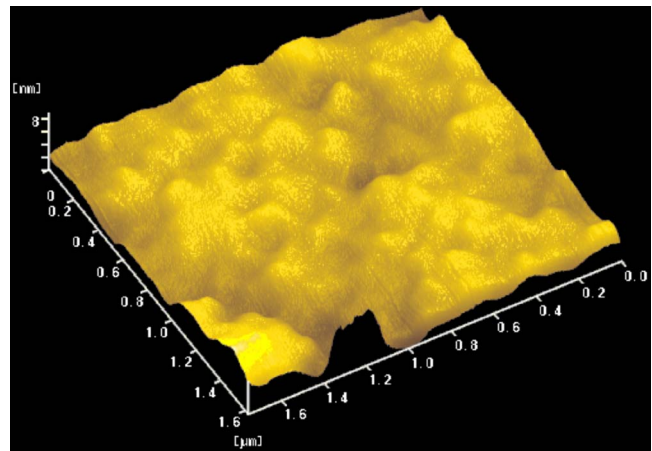


FIG. 5. (Color online) SPM image of SRO thin film grown on LAO substrate.

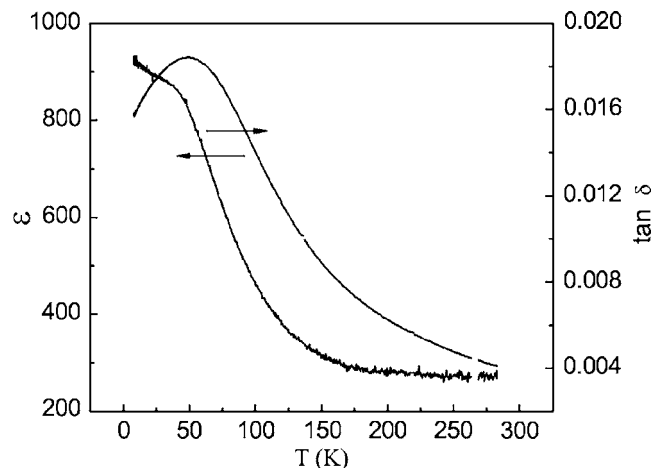


FIG. 6. Temperature dependence of the dielectric constant ϵ and loss tangent $\tan \delta$ of the STO thin films grown on SRO/LAO. The measurements were performed at 1 kHz with a signal level of $0.2 V_{\text{rms}}$.

higher than that observed in STO single crystal. In general, it is impossible to exclude the existence of defects, such as oxygen vacancies, even in high quality epitaxial STO thin films. In STO thin films with defects, one-phonon absorption and phonon scattering on localized phonons near defects may give rise to extra losses. In addition, strain, free carriers, impurity, and interfacial effects are all possible sources of higher loss. Here, although the use of buffer layer SRO may reduce the strain and interfacial effects, earlier HRTEM studies indicated that some defects propagate through the SRO layer.^{15,16} These defects could reach the STO/SRO interface and give rise to defects in the STO layer. As a result, the formation of dislocations at the interface between STO and SRO serves to relieve the strain. At any rate, the change of any kind of static or dynamic disorder in terms of microstructure and stoichiometry may affect dielectric behavior of STO thin films.

IV. CONCLUSIONS

Heterostructures of SRO/LAO and STO/SRO/LAO were prepared. The effects of the microstructures and strain of perovskite ruthenate and titanate films on their magnetic and dielectric properties were studied. Significant anisotropic magnetotransport properties were observed in SRO films.

Thin films of perovskite titanates show the dielectric properties substantially differing from those in corresponding single-crystal materials.

ACKNOWLEDGMENTS

This work was supported by a grant from the Research Grants Council of Hong Kong (CERG under Project No. PolyU7025/05P). The authors would like to acknowledge Z. Luo, W. Huang, and Z. P. Wu for their assistance in morphology measurement.

- ¹C. L. Chen, Y. Cao, Z. J. Huang, Q. D. Jiang, Z. Zhang, Y. Y. Sun, W. N. Kang, L. M. Dezaneti, W. K. Chu, and C. W. Chu, *Appl. Phys. Lett.* **71**, 1047 (1997).
- ²Y. Kumura, T. Ozaki, H. Kanaya, O. Hidaka, Y. Shimojo, S. Shuto, Y. Yamada, K. Tomioka, K. Yamakawa, S. Yamazaki, D. Takashima, T. Miyakawa, S. Shiratake, S. Ohtsuki, I. Kunishima, and A. Nitayama, *Solid-State Electron.* **50**, 606 (2006).
- ³R. A. Rao, Q. Gan, and C. B. Eom, *Appl. Phys. Lett.* **71**, 1171 (1997).
- ⁴F. He, B. O. Wells, Z. G. Ban, S. P. Alpay, S. Grenier, S. M. Shapiro, W. Si, A. Clark, and X. X. Xi, *Phys. Rev. B* **70**, 235405 (2004).
- ⁵M. Mlynarczyk, K. Szot, A. Petraru, U. Poppe, U. Breuer, R. Waser, and K. Tomala, *J. Appl. Phys.* **101**, 023701 (2007).
- ⁶J. Sakai, N. Ito, S.-I. Ito, K. Takahashi, and H. Funakubo, *Appl. Phys. Lett.* **89**, 242115 (2006).
- ⁷G. Herranz, F. Sanchez, N. Dix, D. Hrabovsky, I. C. Infante, J. Fontcuberta, M. V. García-Cuenca, C. Ferrater, and M. Varela, *Appl. Phys. Lett.* **89**, 152501 (2006).
- ⁸J. H. Hao, J. Gao, and H. K. Wong, *Thin Solid Films* **515**, 559 (2006).
- ⁹J. H. Hao, J. Gao, Z. Wang, and D. P. Yu, *Appl. Phys. Lett.* **87**, 131908 (2005).
- ¹⁰J. H. Cho, Q. X. Jia, X. D. Wu, S. R. Foltyn, and M. P. Maley, *Phys. Rev. B* **54**, 37 (1996).
- ¹¹L. M. Wang, H. E. Horng, and H. C. Yang, *Phys. Rev. B* **70**, 014433 (2004).
- ¹²A. T. Zayak, X. Huang, J. B. Neaton, and K. M. Rabe, *Phys. Rev. B* **74**, 094104 (2006).
- ¹³J. C. Jiang, X. Q. Pan, and C. L. Chen, *Appl. Phys. Lett.* **72**, 909 (1998).
- ¹⁴D. B. Kacedon, R. A. Rao, and C. B. Eom, *Appl. Phys. Lett.* **71**, 1724 (1997).
- ¹⁵J. S. Wu, C. L. Jia, K. Urban, J. H. Hao, and X. X. Xi, *J. Mater. Res.* **16**, 3443 (2001).
- ¹⁶J. S. Wu, C. L. Jia, K. Urban, J. H. Hao, and X. X. Xi, *Philos. Mag. A* **82**, 65 (2002).
- ¹⁷G. Herranz, B. Martínez, J. Fontcuberta, F. Sánchez, M. V. García-Cuenca, C. Ferrater, and M. Varela, *Appl. Phys. Lett.* **82**, 85 (2003).
- ¹⁸R. V. Chopdeka, Y. Takamura, and Y. Suzuki, *J. Appl. Phys.* **99**, 08F503 (2006).
- ¹⁹J. Hao, W. Si, X. X. Xi, R. Guo, A. S. Bhalla, and L. E. Cross, *Appl. Phys. Lett.* **76**, 3100 (2000).
- ²⁰A. A. Sirenko, C. Bernhard, A. Golnik, A. M. Clark, J. Hao, W. Si, and X. X. Xi, *Nature (London)* **404**, 373 (2000).